International Journal of Biological Macromolecules 355 (2026) 151432

Contents lists available at ScienceDirect

International Journal of Biological Macromolecules

journal homepage: www.elsevier.com/locate/ijbiomac

Model investigation of a consecutive dye uptake and release process by using a bilayered chitosan-mesoporous silica nanocoating system

Péter Márton [a,b], Simon Titkó [a,c], András Marton [c], Bálint Fodor [c], Péter Basa [c], Gergely Stankovits [a], Benjámin Gyarmati [a], János Rohonczy [d], Tamás Szabó [e], Dániel Zámbó [a], Zoltán Hórvölgyi [a,*]

[a] Department of Physical Chemistry and Materials Science, Faculty of Chemical Technology and Biotechnology, Budapest University of Technology and Economics, Műegyetem rkp. 3., H-1111, Budapest, Hungary
[b] Institute of Technical Physics and Materials Science, HUN-REN Centre for Energy Research, Konkoly-Thege Miklós út 29-33, H-1121, Budapest, Hungary
[c] Semilab Semiconductor Physics Laboratory Co. Ltd., Pirelle Kornélia u. 2., H-1117, Budapest, Hungary
[d] Department of Inorganic Chemistry, Institute of Chemistry, Faculty of Science, Eötvös Loránd University, Pázmány Péter stny. 1/A, H-1117, Budapest, Hungary
[e] Functional Interfaces Research Group, Institute of Materials and Environmental Chemistry, HUN-REN Research Centre for Natural Sciences, Magyar tudósok körútja 2., Budapest, 1117, Hungary

ARTICLE INFO

Keywords:
Chitosan
Mesoporous silica reservoir
Bilayer nanocoating
Rhodamine 6G
Uptake and release

ABSTRACT

Two-layer model systems were designed by covering a 130 nm thick mesoporous silica coating (30% porosity, 1.8 nm average pore radius) with a 470 nm thick chitosan coating (degree of acetylation 18–19%) to study the accumulation and release of a cationic model molecule (rhodamine 6G dye). The coatings were impregnated in the aqueous solution of the dye (pH 6.0, 7.4 and 8.8, 12 °C, 22 °C and 32 °C) to study the effect of electrostatic interactions and morphology on the dye uptake. The accumulation of dye molecules was examined in terms of the pseudo-first-order and pseudo-second-order kinetic model, while the release (at pH 7.4, 25 °C) in terms of the Korsmeyer-Peppas and Higuchi model. The release exponents (0.43–0.71) of the Korsmeyer-Peppas model revealed the significance of an interaction of the impregnation solution with the silica pore wall during dye uptake. According to the Higuchi model, a straight line with a higher and a lower slope could be fitted to the experimental points in the first ("fast rate") and second ("slow rate") stages of the process. Interestingly, the slope values and their differences significantly depended on the conditions of dye uptake: impregnation at alkaline pH not only increased the uptake but also resulted in faster release.

1. Introduction

Stimuli-responsive hybrid nanocarriers represent new frontier in advanced biomedical research, offering precise control over the drug release. These systems can be formed from polymer hydrogels [1–4] or porous inorganic oxides [5,6], both of which enable controllable and extended release of the accumulated molecules over time. A good example of the first is chitosan, which is produced from chitin by partial alkaline deacetylation [7]. Due to its biocompatibility and antibacterial behaviour, it is an ideal material in medicine [8,9], and its applicability in controlled release systems is enhanced by its pH-responsive behaviour due to its free amino groups [10]. An example of the second type is mesoporous silica, which is widespread due to its biocompatibility, high specific surface area and effective adsorption of drugs [11,12]. Additionally, the surface chemistry and porosity of silica are suitable to modification by the solvent environment and drug-matrix interactions [13], justifying its application as a reactive reservoir. By combining the advantages of the inorganic oxides (mechanical stability, high surface area) with the responsive behaviour of organic polymers, synergistic effects can be achieved: the mesoporous silica base coated with a polymer layer, can provide an even more extended and controllable release profile [14]. This combination of inorganic and organic materials is studied in various forms and sizes such as nanoparticles [15], microspheres [16] and nanocoatings [17].

* Corresponding author.
E-mail addresses: marton.peter@vbk.bme.hu (P. Márton), simontitk@gmail.com (S. Titkó), andras.marton2@semilab.hu (A. Marton), balint.fodor@semilab.hu (B. Fodor), peter.basa@semilab.hu (P. Basa), stankovits.gergely@vbk.bme.hu (G. Stankovits), gyarmati.benjamin@vbk.bme.hu (B. Gyarmati), janos.rohonczy@ttk.elte.hu (J. Rohonczy), szabo.84.tamas@ttk.hu (T. Szabó), zambo.daniel@ek.hun-ren.hu (D. Zámbó), horvolgyi.zoltan@vbk.bme.hu (Z. Hórvölgyi).

https://doi.org/10.1016/j.ijbiomac.2026.151432
Received 12 October 2025; Received in revised form 19 February 2026; Accepted 12 March 2026
Available online 14 March 2026

Mesoporous silica is usually loaded with the drug before the polymer layer is applied. Nevertheless, several authors observed that a significant part of the active ingredient was lost or damaged during the washing steps after impregnation or during the deposition of the polymer layer [18,19]. A possible solution to the problem is the impregnation of the silica base already coated with the polymer layer [20,21]. In this case the polymer layer can also protect the reactive reservoir against the aforementioned structural change (erosion processes) during the impregnation.

In this study, the mechanism of adsorption and release in a planar a mesoporous silica (reactive reservoir) – chitosan (pH-responsive layer) nanocoating system is investigated, distinguishing the present work from previous nanoparticle-based approaches. Rhodamine 6G (R6G) was selected as a model molecule due to its well-defined physicochemical properties, high sensitivity for detection via UV–Vis spectroscopy, (which allows for precise monitoring of release kinetics) and effective adsorption from its aqueous solution at the silica pore surfaces due to its cationic nature [17,22,23]. Furthermore, R6G serves as a reliable structural analog for cationic, polycyclic drugs, most notably doxorubicin due to its rigid aromatic backbone and cationic charge under physiological conditions, resulting in similar adsorption and diffusion characteristics within the nanocoating system [24,25]. This similarity allows R6G to effectively simulate the loading and release behaviour of these type of chemotherapeutics during the formulation optimization phase.

Our hypothesis is that by utilizing the pH-responsivity and protective nature of the chitosan coating not only the loading of the reactive reservoir, but also the release kinetics of the model ingredient can be tuned by the impregnation conditions. To the best of our knowledge, the accumulation and release kinetics within a planar two-layer (chitosan-silica) nanocoating system have not yet been investigated, particularly concerning the influence of impregnation conditions. This study addresses this critical gap by systematically evaluating how pH and temperature during the loading phase affect the equilibrium adsorption and subsequent release profiles. Such an approach offers novel insights into the fine-tunability of the delivery process, exploring the interplay between electrostatic interactions and morphological changes – an aspect largely overlooked in previous studies despite its relevance for implantation technologies [26,27].

2. Methods

2.1. Reagents

Chitosan powder (Medium molecular weight: 200–300 kDa, 75–85% degree of deacylation), phosphoric acid (85%, f.a.), boric acid (99.5% f. a.), Pluronic P123 (triblock poly(ethylene glycol)–poly(propylene glycol)–poly(ethylene glycol)), sodium chloride (99.5%, f.a.) and rhodamine 6G dye (95% f.a.) were purchased from Merck (Germany). Isopropanol (99.7%, f.a.), absolute ethanol (99.8%, a.r.) and tetraethyl orthosilicate (TEOS, 98% a.r) were provided by Reanal (Hungary). Acetic acid (99.8% f. a.) was purchased from Lachner (Czech Republic), hydrochloric acid (37% f.a.) and sulfuric acid (96%, f.a.) from Carlo Erba (Italy), and NaOH from Fischer Chemical (USA). All chemicals were used without any further purification. Ultrapure water (specific electrical resistance: >18.2 MΩcm) was made with an Adrona system (Adrona Integrity+).

2.2. NMR spectroscopy

In order to determine the degree of acetylation of the chitosan used in the measurements, NMR spectroscopic studies were performed according to the method by Heux et al. [28]. ^{13}C CP-MAS NMR spectra were recorded by Bruker Avance-III 500 MHz NMR spectrometer at 11.744 T using ZrO rotor and 4 mm BB/1H MAS probe. 2048 data points were received with 5 s relaxation delay at 125.77 MHz in a 300 ppm wide spectral window. Standard Bruker *cp* cross polarization pulse sequence was used with ramp90100.100 shaped proton CP pulse and 2 ms contact time. The integral values were calculated from the 8 K spectrum points obtained after Fourier transformation.

The degree of acetylation (*DA*) of the polymer was determined by the ratio of the integral of the acyl carbon signal (I_{CH3}) at about 25 ppm, and the sixth of the integral of the C1-C6 signals (D-glucopyranosyl ring, I_{C1-6}) in the range of 50 ppm to 120 ppm (Eq. 1) [29].

$$DA = \frac{I_{CH_3}}{\frac{1}{6} \bullet \sum I_{C1-6}} \bullet 100\ [\%] \tag{1}$$

2.3. Potentiometric titration

The degree of acetylation of the polymer was also determined by potentiometric titration. The measurement was carried out with the method of Balázs and Sipos [30]. 0.1004 g chitosan and a calculated amount of HCl were measured into a 25 mL flask and diluted with approximately 20 mL ultrapure water. The mixture was stirred overnight at room temperature, until all of the chitosan dissolved. The solution was transferred into a 100 mL flask, a calculated amount of solid NaCl was added, and the solution was brought to volume. The stock solution thus became 0.010 M for HCl, 0.1 M for NaCl, and approximately 1 mg/mL for chitosan. The NaOH solution with a nominal concentration of 0.1 M was made by dissolving 2.000 g NaOH in 500 mL ultrapure water. The solution was factored with a 0.100 M standard HCl solution (diluted from 1.000 M HCl (Titrisol®, Merck). A single-junction glass pH electrode (Metrohm, Electrode Plus, pH range: 1–13, filled with 3 M KCl) was calibrated using commercial pH buffers (Merck Certipur® buffer solutions with pH = 4.01; 6.86 and 9.18). Titrations were carried out at constant temperature (25 ± 1 °C), in an inert atmosphere (N_2 gas bubbling). During the titrations, a total volume of 20 mL of initially acidic solution was titrated with NaOH using an auto-titrator (Metrohm 808 Titrando, Tiamo, version 1.2). "Dynamic Equivalence Point Titration" mode with custom parameters (maximum signal drift: 3 mV min^{-1}, min. Waiting time: 5 s, max. Waiting time: 40 s after each addition, min. Volume increment 10 μL, max. Volume increment 50 μL, finish at pH = 11.5) was used.

The two inflexion points (V_1 corresponding to neutralization of HCl, and the V_2 corresponding to neutralization of the ammonium groups from chitosan) were determined by plotting the second derivative of pH versus volume of NaOH solution. The *DA* was calculated with Eq. 2 [31,32].

$$DA\ [\%] = \left(1 - \frac{2.03 \bullet \Delta V}{m + 0.0042 \bullet \Delta V}\right) \bullet 100 \tag{2}$$

where ΔV is the difference of V_2 and V_1, m is the weight of the chitosan in 20 mL solution and 2.03 and 0.0042 are constants derived from the molecular weight of chitin residue and acetyl group.

When the degree of protonation (α) of the chitosan is calculated, it must be considered that the protonated amino groups of the polymer during titration behave as weak acid and are capable of self-dissociation. For this reason, the true degree of protonation can be approximated using Eq. 3 [33,34].

$$\alpha = \alpha' + \frac{[H^+]}{C} \tag{3}$$

where α' is the degree of protonation directly deduced from the amount of added NaOH, $[H^+]$ is the concentration of free protons (calculated from pH) and C is the concentration of glucosamine residues. The pKa value of the polymer was calculated by interpolating the pH value of the titration curve for $\alpha = 0, 5$ [35]. The results were calculated from the titration curve of four replicate samples ($n = 4$).

2.4. Coatings preparation

Before the deposition of the coatings, the glass substrates (Menzel-Gläser, Germany) were cleaned with aqueous detergent solution (5 *w*/w %), sulfuric acid solution (10 w/w %), isopropanol and ultrapure water.

Since Na^+ and Ca^{2+} ions can diffuse from the glass substrate into the porous silica layer and affect the structure and surface charge of it [36], a compact silica (SiO_2) protective layer was first deposited on the glass substrate. A precursor sol was made by mixing 38.5 mL absolute ethanol, 31 mL TEOS and 10 mL 0.1 M hydrochloride acid, and stirring it for 1 h, then used for dip-coating after one day aging. For the mesoporous silica ($pSiO_2$) layers, two solutions (one with 2 g P123 and 22 mL absolute ethanol, and one with 4 mL 0.1 M hydrochloride acid, 8.8 mL TEOS and 22 mL absolute ethanol) were stirred separately for 30 min, then combined and stirred together for another 30 min. The deposition of the silica coatings was performed with a device made by Plósz Mérnöki Iroda kft. (Budapest, Hungary) with a withdrawal speed of 6 cm/min at 25 °C. At the first step, the protective SiO_2 layer was formed on the substrates, then the samples were calcinated at 450 °C for 30 min in a Nabertherm B180 furnace. At the second step, the $pSiO_2$ coating was deposited and the calcination time was 60 min at 480 °C [37].

For the chitosan (CS) layers, a 1% (*w*/w) solution of the polymer was made by carefully sprinkling 0.5 g chitosan powder onto the surface of a mixture of 49 mL ultrapure water and 500 μL acetic acid. The solution was stirred overnight, then the insoluble particles were removed by centrifugation (Hermle Z36HK device, 30 min at 4000 rpm) and decantation. The coatings were formed at 25 °C by the dip-coater mentioned above with a withdrawal speed of 5 cm/min to the bare and SiO_2/$pSiO_2$-coated glass substrates. The samples dried overnight at room temperature.

Since the function of the SiO_2 layer is only protection, but it does not affect the dye uptake, the samples with the chitosan coated silica layer are referred as bilayer systems (since there are two "active" layers on them) and the samples with only $pSiO_2$ or CS layers are referred as monolayer systems.

2.5. UV–vis spectroscopy

The thickness and refractive index of the CS monolayers were determined by UV–visible spectroscopy. The transmittance spectra of the samples were measured with an Analytik Jena Specord 200 UV–Vis spectrophotometer in the 350–1100 nm wavelength range with 1 nm resolution, and 10 nm/s scan rate. The above parameters of the monolayer CS coatings were determined by a thin-layer optical model (Hild-method) [38,39] fitted to the transmittance spectra. The optical model assumes one homogeneous layer with no absorption on each side of the substrate. The thickness and refractive index were calculated from the fitted values of twelve replicate samples ($n = 12$).

2.6. Spectroscopic ellipsometry

To characterize the optical properties of the bilayer samples, i.e. to determine the thickness and refractive index of each layer a Semilab SE-2000 Spectroscopic Ellipsometer was used. The measurements were performed in the wavelength range of 250–975 nm, at three angles of incidence (65°, 60°and 55°), close to the center of the samples. Reference values were used for the refractive index of the bare glass, while a Sellmeier dispersion law was fitted for the SiO_2, $pSiO_2$ and CS layers. The thickness and refractive index were calculated from the fitted values of twelve replicate samples (n = 12).

2.7. Ellipsometric porosimetry

To determine the open porosity and the pore size distribution of the $pSiO_2$ layer, ellipsometric porosimetry measurements were performed with a Semilab PS-2000 Ellipsometric Porosimeter. Adsorption isotherms of toluene (Carlo Elba, HPLC grade) were measured at 30 °C in the relative pressure ranges of 0.0005–0.999. Ellipsometric measurements were taken in the wavelength range of 250–975 nm, with a fixed angle of incidence of 60°. The samples were placed on a hot plate and heated at 150 °C for 15 min before loading them into the porosimeter. The samples were evacuated, flushed with nitrogen, allowed to cool down for 30 min, then evacuated again, before performing the measurements.

2.8. Scanning electron microscopy and EDS measurements

For scanning electron microscopy (SEM) SiO_2, SiO_2/$pSiO_2$ and SiO_2/$pSiO_2$/CS coating systems were applied to silicon substrate (Double Side Polished, 100, Siegert Wafer GmbH, Germany) to avoid electrostatic charging from the glass substrate during the measurement. The silicon substrates were cleaned with isopropanol and ultrapure water, then plasma treated for 5 min for increasing the polarity of the surface for better wettability by the precursor sols. For the treatment, a Smart-Plasma 10 laboratory plasma system was used (Plasma Technology GmbH, generator: 40–100 kHz, 300 W) at 50% (150 W) power and 15 Pa pressure. Cross-section electron microscopy and elemental mapping of the coatings was performed using a Zeiss LEO 1540-XB scanning electron microscope equipped with an Oxford Instruments UltimMax 40 detector operated at 5 keV acceleration voltage after the samples were carefully scratched and broken. AZtecOne analysis software was used for the processing, evaluation and visualisation of the EDS data.

2.9. Sample impregnation with R6G dye molecules

The impregnation was carried out in the 10^{-4} M R6G aqueous solutions at different pH (between 6.0 and 8.8) and at different temperatures (12 °C, 22 °C and 32 °C), provided by a Hermle Vibramax 100 laboratory shaker equipped with a Hermle Incubator 1000 heater, and a POL-EKO-APARATURA ILW 115 Cooled incubator. The solutions were made by adding 335 μL 1.5^{-2} M dye solution into 50 mL Britton-Robinson (BR) buffer solution. The BR buffer was prepared using an acidic component (0.04 M boric acid, 0.04 M phosphoric acid, 0.04 M acetic acid mixture). The desired pH was achieved by adding 0.2 M NaOH solution (basic component) to the mixture and constantly monitoring the pH with a glass combined electrode (Mettler Toledo InLab Micro) connected to a Sartorius PB-11 pH meter. During impregnation, the samples were placed in the prepared dye solution in a slide staining trough in a vertical position, so that the solution was in contact with the coating on both sides. The trough was not shaken or stirred during the process. After 10 min of impregnation, the samples were taken out, rinsed with ultrapure water and dried at room temperature. After recording the absorbance spectra of the dry samples, they were impregnated for another 10 min, rinsed, dried and measured, and so on, until the total impregnation time reached 120 min. The absorbance values at 527 nm were corrected by the absorbance measured before impregnation, and normalized with the thickness of the layer containing the dye to eliminate the error due to the change in layer thickness [37]. The results of the dye uptake were calculated from the data of 3 replicate samples ($n = 3$).

The adsorption kinetics was studied by fitting model functions to the normalized absorbance values, which is essential for the characterization of the adsorption efficiency (equilibrium adsorbed amount and time-dependency). The most commonly used models for the study of dye adsorption from aqueous media on silica and similar mesoporous sorbents are the pseudo-first-order (PFO) and pseudo-second-order (PSO) kinetic models given below as Eq. 4 and 5 respectively [13,40].

$$A_{norm} = A_e \bullet \left(1 - e^{-k_1 t}\right) \tag{4}$$

$$A_{norm} = \frac{A_e^2 k_2 t}{1 + A_e k_2 t} \tag{5}$$

where A_{norm} [nm^{-1}]is the normalized absorbance of the sample after a given impregnation time t [min], A_e [nm^{-1}] is the normalized absorbance at equilibrium, and k_1 [min^{-1}] and k_2 [nm/min] are the rate constants of the PFO and PSO models respectively.

2.10. Rhodamine 6G release experiments

The dye release experiments were carried out at 25 °C by placing an impregnated bilayer sample in 25 mL of BR buffer with a pH of 7.4 (standard ambient temperature and physiological pH). With continuous gentle stirring, the spectrum of the buffer solution was recorded every minute for 6 h in the 350–800 nm wavelength range using an Agilent FA-VAR00-AP0X optical fiber probe connected to an Agilent Cary 60 UV–Vis spectrophotometer. The spectrum was corrected with the spectrum of the clean buffer solution, and the absorbance values measured at 527 nm were used to evaluate the data.

To determine the total amount of dye in the samples, after a 6-h measurement they were stored together with the buffer in 30 mL containers for another 162 h (one week in total) at 25 °C. Then the samples were taken out, rinsed with ultrapure water and dried at room temperature. The absorbance spectra of the samples were recorded proving that the whole amount of dye has been released. The spectra of the buffers were also recorded, and the measured absorbance at 527 nm considered as 100% and used to normalize the data from the release experiments. To calculate the concentration and exact amount of dye, a calibration curve was used, for which a series of calibration solutions were prepared with the pH 7.4 BR buffer in the concentration range between 0.5 and 10 μM. The results were calculated from the data of 3 replicate samples ($n = 3$).

2.11. Additional measurements

For the detailed description of the molecular weight determination of the chitosan polymer, the infrared spectroscopy and the surface zeta potential measurements, see Section A1 in Appendix.

2.12. Statistical analysis

Mean with standard deviation and ANOVA test ($p < 0.05$) were used for the statistical analysis using OriginPro 8.6 software (OriginLab Corporation, Northampton, MA, USA). Significant differences in the figures are marked with lowercase letters above the data points, where the different letters mean significantly different values (compact letter display).

3. Results and discussion

3.1. Characterization of the model system

To interpret the results of the dye uptake tests, it is essential to know the properties of the investigated bilayer coating system precisely, because the thickness of the coatings, the properties of the CS polymer and the porosity of the $pSiO_2$ can significantly affect the amount of dye adsorbed and the kinetics of adsorption and release. The thickness, refractive index and porosity of the coatings were studied by UV–Vis spectroscopy and spectroscopic ellipsometry, while the DA and pK_a value of the chitosan were studied by NMR spectroscopy and potentiometric titration.

3.1.1. Thickness and pore structure of the layers

It could be observed with the naked eye that the coatings after each deposition were transparent and homogenous (photographs of the samples are provided in Fig. A1 in Appendix). The thickness and refractive index of coatings were measured with thin layer optical analysis (by fitting an optical model to the spectra obtained by UV–Visible spectroscopy and spectroscopic ellipsometry). The fitted results for the systems are summarized in Table 1 (there are CS coatings deposited as the top layer of the bilayer systems and as monolayers on glass, listed in the last two rows of the table, respectively). The small relative standard deviation of the results (3–4% for thicknesses, while 0.5% for refractive indices) proves the good reproducibility of the nanolayers with this technique.

There is a small difference between the thickness and the refractive index of the CS coatings that are monolayers and part of the bilayer system, which is probably a consequence of the difference in the chemical and morphological properties of the surfaces underneath (glass or $pSiO_2$) during coating deposition.

The recorded transmittance spectra of the system after each coating deposition can be seen in Fig. 1d. The spectra of the first two layers (SiO_2 and $pSiO_2$) are above the spectrum of the bare glass substrate, because the refractive index of these coatings is lower than that of glass (approximately 1.52) [41]. The refractive index of the CS coating is higher, and the transmittance drops below that of the bare substrate, and due to the notable increase in the thickness of the system, the change in transmittance due to thin-layer interference becomes more significant.

The structure and thickness of the coatings were investigated using scanning electron microscopy as well. The cross-section SEM images of the SiO_2, SiO_2/$pSiO_2$ and SiO_2/$pSiO_2$/CS coating systems on silicon substrate are provided in Fig. 1a, b and c respectively, where the compact and porous structure of the SiO_2 and $pSiO_2$ coatings are visible. From these images, the thickness of the individual layers can also be determined, and the values are in good agreement with the data in Table 1 (182 nm, 132 nm and 505 nm respectively for the three layers).

The elemental analysis of the area shown in Fig. 1c was also performed using EDS (the obtained spectrum is shown in Fig. A2, while the elemental maps are shown in Fig. A3 in the Appendix). The three coating layers are clearly separated in the element maps: the substrate is pure silicon and the SiO_2 and $pSiO_2$ coatings contain only silicon and oxygen. The intensity of the signal of these elements reflects the structural differences (i.e. compact and porous coating). Moreover, the elemental map of the CS coating is dominated by carbon and nitrogen.

The chemical structure and composition of the coating layers were also confirmed by ATR-FTIR measurements. The obtained spectra (in Fig. A4) and their interpretation can be found in the Appendix.

Based on the results of spectroscopic ellipsometry, the porosity of the $pSiO_2$ coating is 30 ± 1%, which decreases slightly when the CS coating is applied, because the CS solution penetrates the pores and after drying, the polymer fills about 18 ± 3% of them (calculated from multilayered Bruggeman effective medium approximation-based model). This porosity value is in good agreement with that obtained from ellipsometric porosimetry (see the highest y-value of the isotherm in Fig. 1e). Based on the results, the specific surface area of the coating was also estimated: considering the excluded surface area of a single toluene molecule as 0.55 nm^2 [41], the resulting specific surface area was 929 ± 3 m^2/cm^3.

3.1.2. Pore size distribution of the $pSiO_2$ layer

The pore system of the $pSiO_2$ layer was characterized by

Table 1
Thickness and refractive index values for each layer in the studied systems measured by spectroscopic ellipsometry (SE) or UV–Visible spectroscopy (UV–Vis) (Mean ± standard deviation, $n = 12$, the layers studied by SE are part of the bilayer model system, the data were determined by evaluating the spectrum of the entire system).

Method	Coating	Thickness [nm]	Refractive index [−]
SE	SiO_2	187 ± 4	1.4355 ± 0.0013
	$pSiO_2$ (on SiO_2)	131 ± 5	1.3158 ± 0.0040
	CS (on SiO_2 and $pSiO_2$)	471 ± 15	1.5722 ± 0.0024
UV–Vis	CS (monolayer) on glass	402 ± 15	1.5407 ± 0.0041

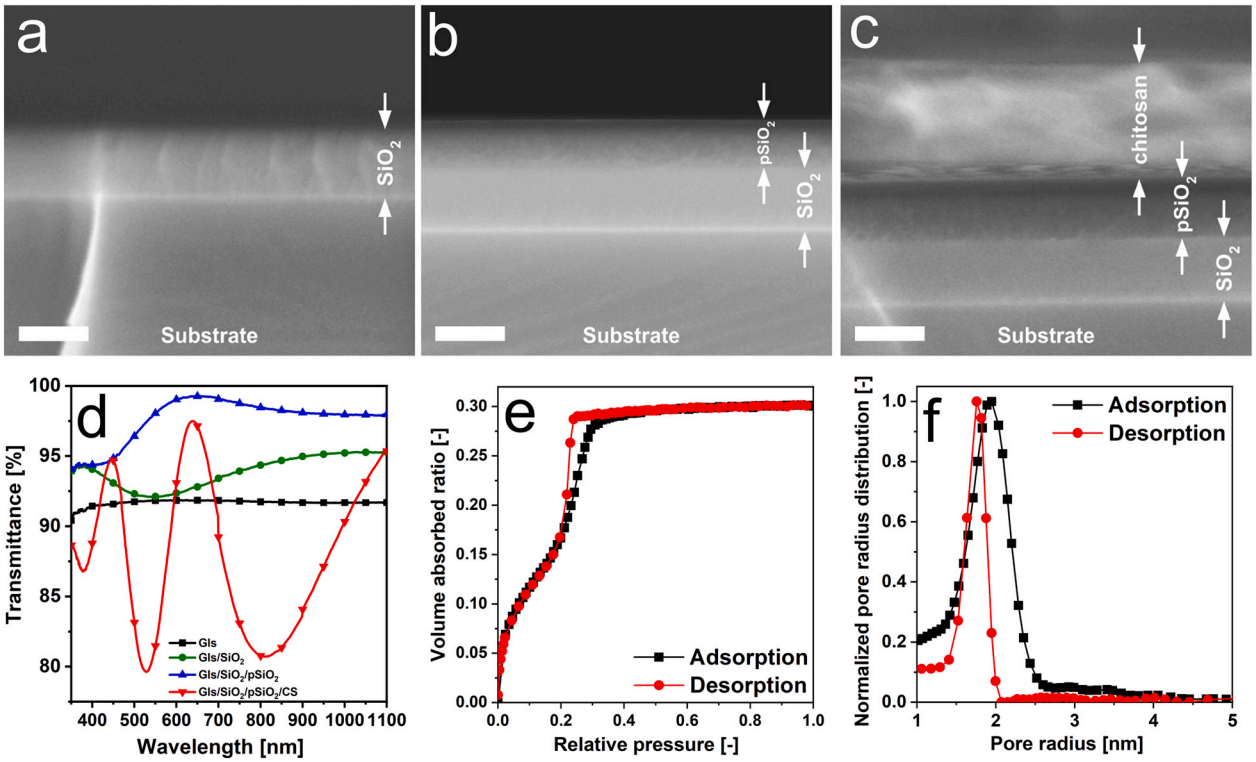

Fig. 1. Cross-section SEM images of the SiO_2 (a), $SiO_2/pSiO_2$ (b) and $SiO_2/pSiO_2/CS$ (c) coating systems on silicon substrate (arrows indicating the different layers, scale bars are 200 nm), transmittance spectra of the studied system on glass substrate after each coating deposition (d) and the adsorption isotherm (e) and calculated pore size distribution (f) of the $pSiO_2$ coating.

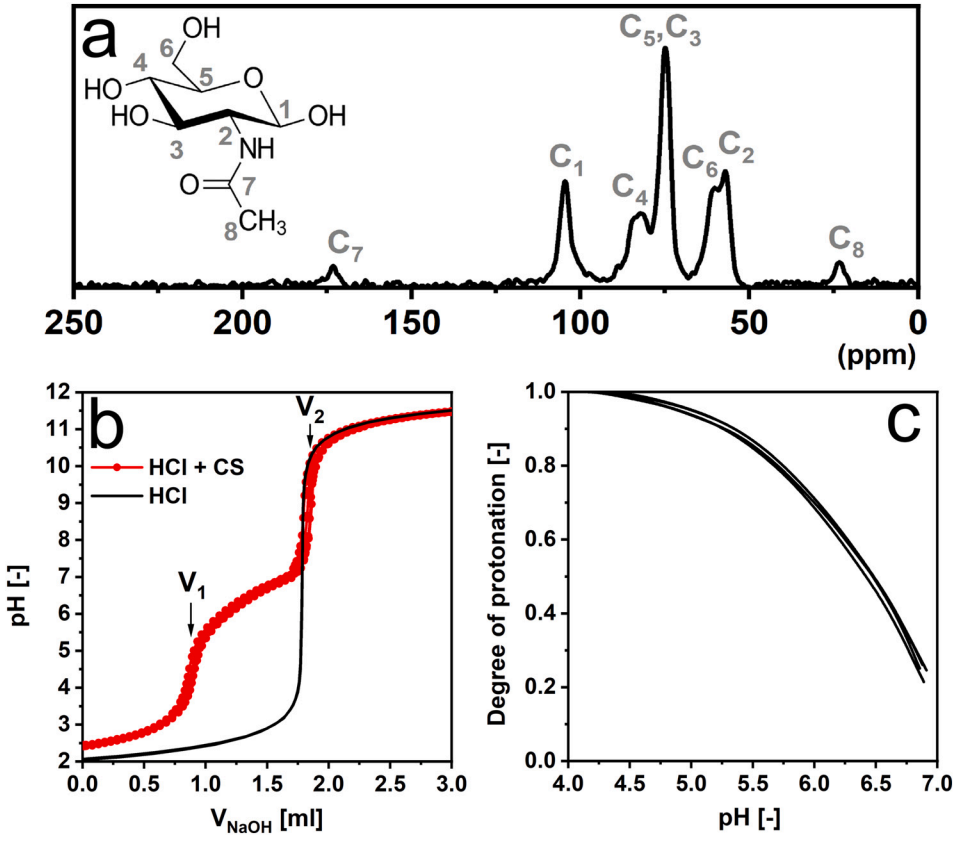

Fig. 2. The solid state C^{13} CP-MAS NMR spectrum of the CS sample with the notation of the peaks (a), the titration curves of the pure and CS-containing HCl solutions (b) and the degree of protonation of the polymer calculated from the titration curves (c) (the multiple curves on b and c correspond to parallel measurements).

ellipsometric porosimetry. Fig. 1e shows the adsorption and desorption isotherm obtained at 25 °C using toluene as adsorptive material. The amount of adsorbed toluene is significant, which means that the pores are open and accessible to adsorbing molecules. Based on the relatively sharp increase in adsorbed volume at low relative pressure values and the sorption-desorption hysteresis, it can be assumed, that the pore system of the coating is mainly composed of mesopores with uniform pore sizes. The pore radius distribution of the system is presented in Fig. 1f. The calculated average pore radius is 1.9 ± 0.1 nm from the adsorption and 1.7 ± 0.1 nm from the desorption isotherms. Using the same sol recipe and template, Kócs et al. previously produced silica nanocoatings with similar pore size distribution [42].

3.1.3. Properties of the chitosan

Since the degree of acetylation (*DA*) of the CS greatly influences the permeability of the nanolayer against charged molecules [37], the first step was to determine its exact value. For this, solid state C^{13} CP-MAS NMR spectroscopy and potentiometric titration were used (the latter also allowed the determination of the pK_a value of the polymer, which is critical for pH-responsiveness). The NMR spectrum of the CS is shown in Fig. 2a (for the notation of the carbon atoms, see Ref. [43]). The *DA* value of the polymer can be calculated from the ratios of the integral values on the NMR spectrum according to Eq. 1. which was found to be 18 ± 1%.

The titration curves of the control HCl solution and the CS-containing HCl solutions are presented in Fig. 2b. While the curve of the pure HCl solution shows only one inflexion, the curves of the CS-containing solutions have two: the one at smaller NaOH volume (V_1) corresponds to the neutralization of HCl, and the one at V_2 corresponds to the neutralization of the quaternary ammonium groups of CS. From the difference of V_1 and V_2, the *DA* value can also be calculated using Eq. 2, which gives 19 ± 1% as a result. The agreement between the *DA* values obtained from the NMR spectrum and the titration curve is reasonable, considering that the difference between these measurement methods can be several percents [44,45]. The result obtained is also within the limits specified by the manufacturer of the polymer (15–25%).

The degree of protonation (α) of the polymer as a function of pH (calculated from the titration curve data using Eq. 3) is shown in Fig. 2c. Since CS precipitated around pH 6.9, and thus Eq. 3 could no longer be used, the curves were only plotted up to this point [30]. The pK_a value of the polymer can be estimated as the pH corresponding with $\alpha = 0.5$. The value calculated this way is 6.46 ± 0.03, which is close to the value found in the literature for chitosan with similar *DA* [46,47]. The molecular weight of the polymer was determined by viscosimetry. The calculated value was 388 kDa (for the viscosity values and the linear fit see Fig. A5 in Appendix).

3.2. Dye accumulation in the model coatings

To investigate the effect of pH and temperature on the adsorption process, the samples were impregnated in 10^{-4} M R6G solutions prepared from Britton-Robinson (BR) buffer solutions (from pH 6.0 to pH 8.8) at 12 °C, 22 °C and 32 °C. This pH range adequately examines the range around physiological pH (7.4) encountered during application without the structural damage of the chitosan coating. The accumulation of the dye was characterized by the absorbance of the samples. To eliminate absorbance differences due to variations in layer thickness, the absorbance of the coatings measured at 527 nm was divided by the layer thickness of either the $pSiO_2$ coating (for bilayer systems and bare $pSiO_2$ coatings) or the CS coating (for CS monolayers).

3.2.1. The effect of pH on the absorbance of the samples

To better understand the phenomenon and the contribution of the individual nanolayers, the impregnation was performed not only on the bilayer model system but also on bare $pSiO_2$ layers (not coated with CS) and on CS monolayers. The normalized absorbance values obtained in this way are summarized as a function of impregnation time and pH in Fig. 3a, b and c (for the bare $pSiO_2$ coatings, CS monolayers and bilayer model systems respectively). The figures show that the normalized absorbance values become constant by the 120th minute, characterizing a close to limitation value of the dye uptake. These values are summarized in Fig. 3d for the studied systems. Note the break on the y-axis, which shows that the CS monolayers absorbed significantly less dye than either the bare $pSiO_2$ or the bilayer systems. This demonstrates that the dye can accumulate in the pores of the $pSiO_2$ coating even when diffusing through the CS layer, due to the strong electrostatic attraction between the pore wall and the dye molecules [17]. To confirm this attraction, the surface zeta potential of the $pSiO_2$ coating was measured at pH 6.0, 7.4 and 8.8. The results are shown in Fig. A6 in the Appendix and clearly demonstrate that the coating surface (and thus presumably the inner wall of the pores) is negatively charged in the tested pH range.

For the bare $pSiO_2$ coatings and CS monolayers (Fig. 3a and b) the close to limitation value of the adsorbed dye increases with increasing pH. In the case of the silica, this can be attributed to the increase of negative charge density at the surface of the pores [48], while in the case of the CS coating the decrease in positive charge density (due to the decreasing number of protonated amino groups) reduces the electrostatic repulsion between the cationic dye and the polymer, thus allowing secondary (attractive van der Waals) molecular interactions to prevail. For the bilayer model systems, the adsorbed amount of R6G also increases with increasing pH. The change in the limitation value of the adsorbed dye in the case of the bilayer systems can be explained by the principle that a coupled equilibrium is established in the system between the dye solution, the CS coating and the $pSiO_2$ coating. The CS coating maintains equilibrium with the R6G solution of constant concentration of 10^{-4} M, and the amount of dye accumulating in the CS is influenced by its charge density. The $pSiO_2$ coating maintains adsorption equilibrium with the concentration (activity) of dye in the CS coating, hence the system behaves at different pH values as if the $pSiO_2$ coating were in equilibrium with dye solutions of different concentrations (activity) [37].

3.2.2. The effect of temperature on the absorbance of the samples

The impregnation of bilayer systems in 10^{-4} M R6G solutions prepared with pH 6.0, 7.4 and 8.8 BR buffers was additionally carried out at 12 °C and 32 °C to study the effect of temperature on the dye accumulation. The results are summarized in Fig. 4a, where different pH values are represented by different colours and temperatures by different markers. The data show that the temperature effect is weak for systems impregnated at pH 6.0, while significant differences can be observed for pH 7.4 and 8.8, where the amount of dye uptake increases with increasing temperature. The only exception is the (pH 8.8, 32 °C) sample, which adsorbs a large amount of dye in the initial stage but releases it as the impregnation progresses. This was also observed in the case of the other samples, which were kept in the dye solution for another 24 h, and the amount of dye adsorbed decreased drastically (data not shown). This is presumably because during prolonged soaking, especially at alkaline pH (near 9) the dissolution of silica may occur, which reduces the specific surface area of the porous coating [48]. This erosion process is of great importance, not only in terms of the amount of dye accumulated, but also in terms of the kinetics of release. The erosion is presumably faster at higher temperature, hence in the case of the sample impregnated at pH 8.8 and 32 °C it could have occurred within the examined 2-h period reducing the amount of adsorbed dye.

In the other cases, the change in the limitation value of adsorbed dye can be explained by the above-described coupled equilibrium (thus the change in the charge density of the CS coating). Cho et al. investigated the degree of protonation of CS as a function of pH and temperature [49]. Based on their results, at a given pH value in the range of 3 to 9, the degree of protonation decreases with increasing temperature. As the degree of protonation decreases, the concentration of dye accumulated in the chitosan coating increases (due to the weaker electrostatic

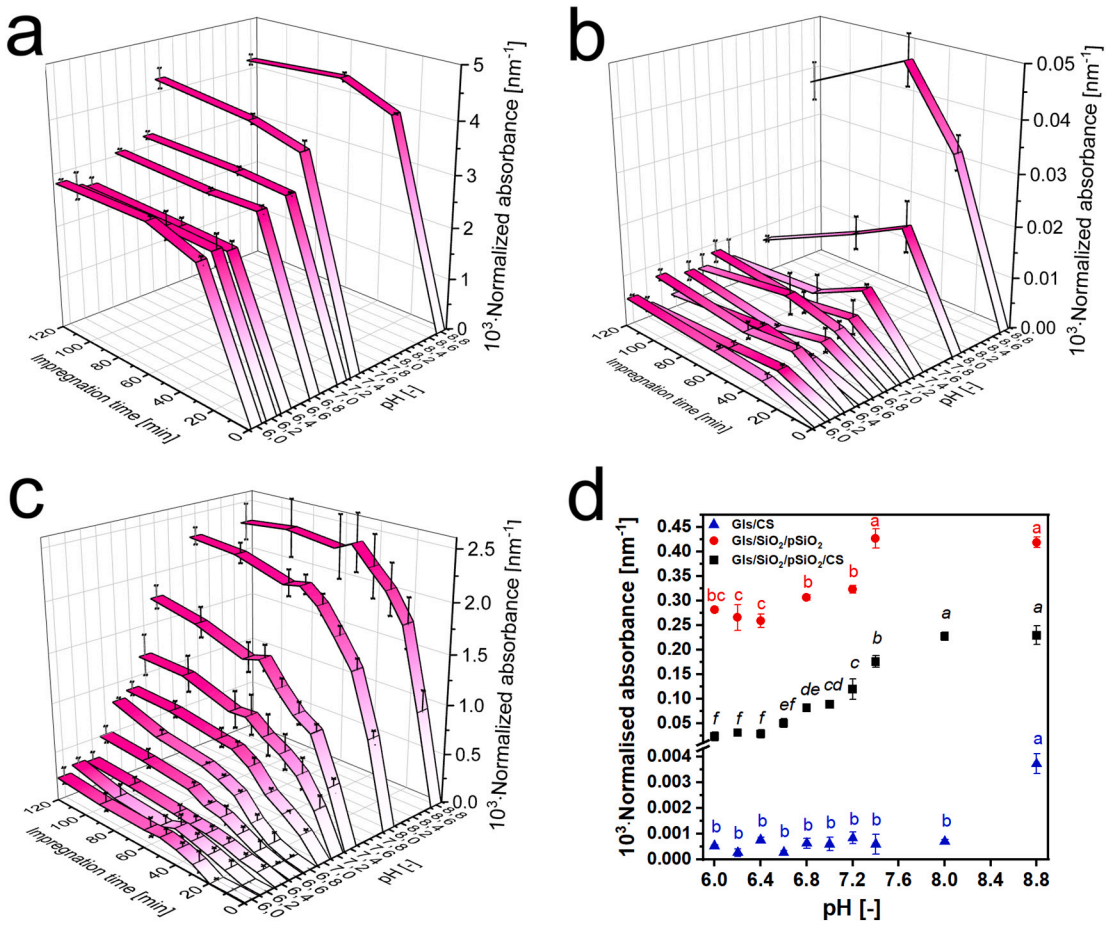

Fig. 3. The normalized absorbance values of the individual coating systems during impregnation at 22 °C in R6G solutions with different pH: Gls/SiO_2/$pSiO_2$ (a), Gls/CS (b), Gls/SiO_2/$pSiO_2$/CS (c) and the values for 120 min (close to limitation values) for all cases examined (d). The absorbances were normalized to the thickness of the pSiO2 layer (a, and b), and to the thickness of the CS layer (c). (Mean ± standard deviation, $n = 3$, the letters above the data points in Fig. 3d indicate significant differences in the three data sets, where a common letter means that the two data values are not significantly different).

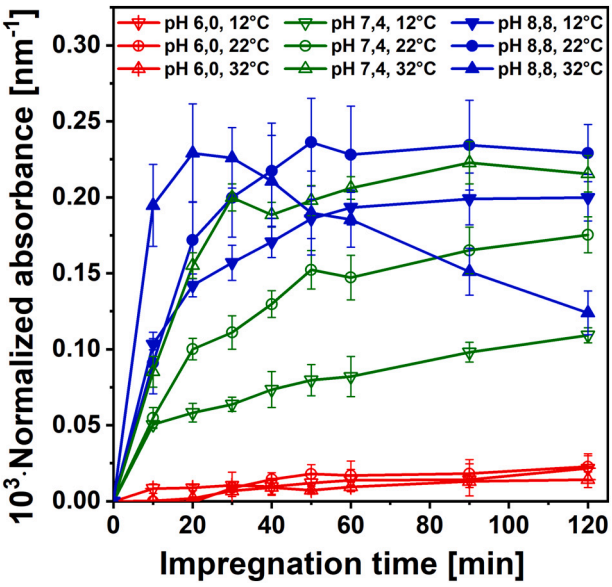

Fig. 4. The normalized absorbance values of the bilayer coating systems during impregnation at different pH and temperature (Mean ± standard deviation, $n = 3$).

repulsion), which results in an increase in the equilibrium amount of dye adsorbed by the $pSiO_2$ layer.

3.2.3. *Sorption kinetics: pseudo-first- and pseudo-second-order models*

To quantify the kinetics of the sorption process, two well-known kinetic models were fitted to the values of normalized absorbances: the pseudo-first-order (PFO) and pseudo-second-order (PSO) models, which are described in Section 2.9. An example for the fitting is shown in Fig. A7 in Appendix. The fitted model parameters are summarized in Table 2, where the correlation factor (R^2) characterizing the fit is also included in each case. Model fit was not possible at the values measured for pH 6.0 due to the small absorbance values measured in the initial stage of impregnation. The correlation factor (R^2) of the PSO model was the same or higher compared to the PFO model in every case, which means that the former model is more suitable for describing the kinetics of R6G adsorption. Huang et al. also observed pseudo-second-order kinetics, when studying the adsorption of cationic dyes (methylene blue and Janus Green B) onto mesoporous silica [50]. However, it should be emphasized that due to the reactive reservoir nature of the $pSiO_2$ coating (possible erosion), a change in mechanism may occur even during the sorption process.

Based on the data of Table 2, the equilibrium amount of dye uptake (A_e value) increases with increasing pH at a given temperature, which can also be attributed to the previously described coupled equilibrium, the lower charge density of the less protonated polymer matrix and the increase in the negative charge density of the pore walls. Similarly, at a given temperature, the dye uptake rate is also higher at more alkaline pH

Table 2
Fitted kinetic model parameters and R^2 values for the adsorption curves plotted in Fig. 4. (PFO: pseudo-first-order model, PSO: pseudo-second-order model, for the meaning and dimension of the parameters, see text) (The fit was not possible in the case of samples impregnated in pH 6.0 solutions, and for samples impregnated at pH 8.8 and 32 °C, the fit was performed using only the data of the first 30 min, Mean ± standard deviation, $n = 3$, the uppercase letters indicate significant differences in each row, where a common letter means that the two data values are not significantly different).

Kinetic models/ Impregnation conditions		Gls/SiO_2/pSiO_2/CS pH = 7.4 T = 12 °C	Gls/SiO_2/pSiO_2/CS pH = 8.8 T = 12 °C	Gls/SiO_2/pSiO_2/CS pH = 7.4 T = 22 °C	Gls/SiO_2/pSiO_2/CS pH = 8.8 T = 22 °C	Gls/SiO_2/pSiO_2/CS pH = 7.4 T = 32 °C	Gls/SiO_2/pSiO_2/CS pH = 8.8 T = 32 °C
PFO	$10^3 \cdot A_e$	100 ± 7^{c}	195 ± 15^{ab}	172 ± 14^{b}	238 ± 27^{a}	217 ± 10^{ab}	230 ± 24^{a}
	$10^3 \cdot k_1$	38 ± 4^{c}	64 ± 6^{b}	38 ± 0^{c}	59 ± 6^{b}	60 ± 2^{b}	194 ± 32^{a}
	R^2	0.897 ± 0.069	0.987 ± 0.004	0.971 ± 0.010	0.955 ± 0.023	0.978 ± 0.004	0.994 ± 0.002
PSO	$10^3 \cdot A_e$	119 ± 9^{c}	224 ± 19^{ab}	214 ± 17^{b}	273 ± 27^{a}	254 ± 12^{ab}	254 ± 22^{ab}
	$10^3 \cdot k_2$	394 ± 16^{b}	388 ± 76^{b}	185 ± 12^{c}	272 ± 34^{b}	288 ± 20^{b}	1475 ± 486^{a}
	R^2	0.938 ± 0.052	0.995 ± 0.004	0.974 ± 0.009	0.965 ± 0.006	0.964 ± 0.012	0.992 ± 0.006

(indicated by the larger k_2 value), which is probably due to faster diffusion through the CS matrix caused by the lower electrostatic repulsion.

3.3. Investigations of dye release

Dye release tests were performed only for the four samples with the highest dye uptake (pH 8.8, 12 °C and 22 °C, and pH 7.4, 22 °C and 32 °C) and for the bare pSiO_2 layer as a reference. Since the primary application of the coating systems would be on the surface of medical implants, physiological pH was used during the release tests. During the experiments, the samples were immersed in BR buffer with pH 7.4 at 25 °C, and the amount of dye released was determined by monitoring the absorbance of the solution at 527 nm. After the six-hour test, the samples were soaked in the buffer for an additional 162 h, during which time the entire amount of dye was released (confirmed by absorbance measurements, data not shown). The coatings maintained their macroscopic integrity and remained attached to the substrate even after this 168 h soaking. Considering the absorbance of the solution measured after this as 100%, the released quantity of R6G in the first six hours can be determined, as shown in Fig. 5a for the selected samples.

Additionally, using the calibration line calculated from the absorbances measured in pH 7.4 buffer (see Fig. A8a in Appendix), the R6G concentration of the solution during release can also be calculated (see Fig. A8b in Appendix). Given the known volume of the buffer (25 mL), the volume and specific surface area of the coating, the amount of R6G accumulated in a sample, its concentration, and the surface coverage after impregnation can be calculated (assuming the excluded surface area of a single R6G molecule as 1.59 nm^2 [51]. The results showed that the dye concentration in the bare pSiO_2 coating was approximately 0.32 M, three orders of magnitude higher than in the impregnating solution (10^{-4} M), which highlights the high efficiency of sorption based on electrostatic interaction [17,52]. The dye covered nearly 35% of the surface area of the coating, presumably because the pore sizes are comparable to the molecular sizes, so perfect coverage was not achieved due to geometric constraints. Douba and coworkers performed R6G sorption experiments on mesoporous silica particles with similar pore size and specific surface area, and based on their results, the dye covers only nearly 20% of the surface area of the pores [53]. The dye concentration for chitosan-coated samples varies between 0.19 and 0.14 M, while the R6G-coverage between 19% and 15% depending on pH and temperature. The detailed calculations and the exact data for the selected samples (Table A1), as well as the calculated sorption capacities according to the A_e values of the PFO and PSO models (Table A2) are summarized in the Appendix.

The release curve of the pSiO_2 coating can be divided into two sections: a shorter initial section, during which a large amount of dye is suddenly released (so-called burst release) and a longer section, during which the release is slower. This type of release profile is typical of mesoporous systems, and can be very important in such cases where a sudden release of a large amount of drug is required, e. g. for acute infections or inflammations [54]. Jarosz et al. assumed that during the burst release, the dye desorbs from the outer surface of the mesoporous coating (which is a faster process), while in the subsequent stage, the dye bound on the internal surfaces of the pores is released, during which both diffusion and desorption are decisive [55].

To study the mechanism of dye release and to more accurately compare individual release curves, it is also advisable to fit kinetic models whose parameters can characterize the release process. One of the most commonly used models is the Korsmeyer-Peppas model, which is described by Eq. 6.

$$\frac{A}{A_\infty} = K_{KP} \bullet t^n \tag{6}$$

where A/A_∞ [−]is the released quantity at time t [s], K_{KP} [s^{-n}] is the rate

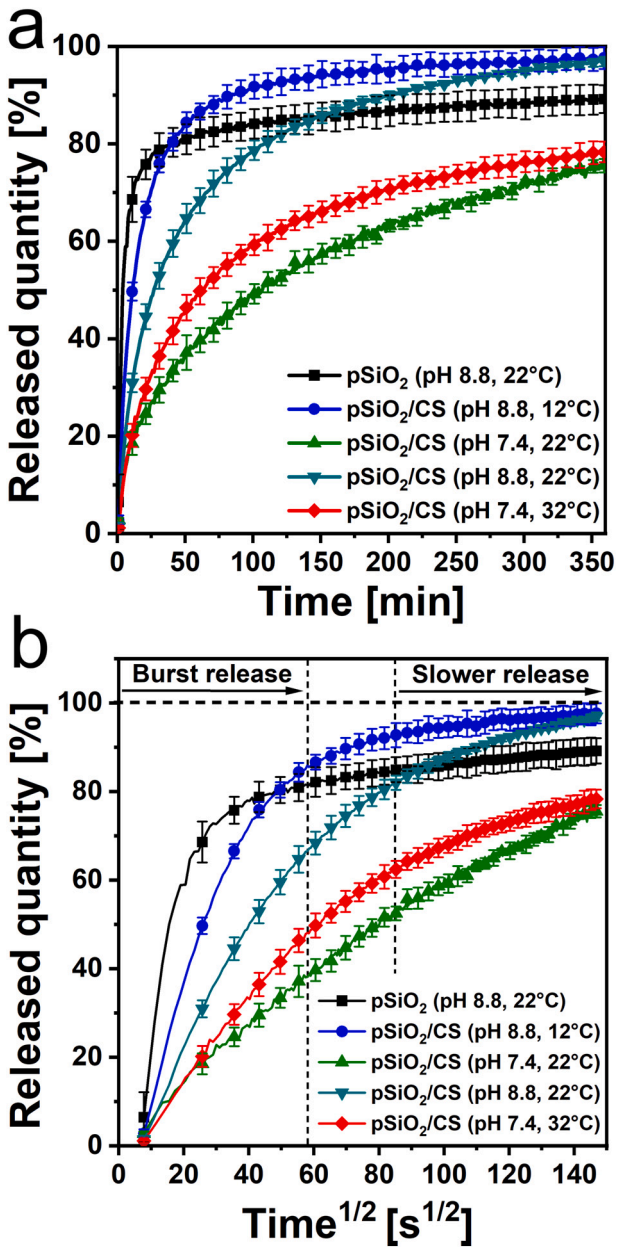

Fig. 5. The amount of dye released during the first six-hour period for the uncoated $pSiO_2$ layer (black squares) and the selected two-layer systems with the highest dye uptake (a), and the same data points as a function of the square root of time, to illustrate the difference in diffusion rate during burst release and slower release phases based on the Higuchi model (b) (the legend shows the conditions of impregnation, Mean ± standard deviation, $n = 3$).

constant and n [−] is the release exponent, the value of which helps to understand the mechanism of the release. When n is 0.5, we can speak of purely diffusion-controlled release, and below 0.5 of quasi-Fickian diffusion. In the case of an exponent between 0.5 and 1, not only diffusion is the determining factor, but also other effects (sorption processes or matrix erosion). The model gives reliable results if the fit is only made up to 60% of the released quantity [56] (see Fig. A9a in Appendix). If complete diffusion control is achieved in the system, the well-known equation developed by Higuchi can be applied [57] (Eq. 8).

$$\frac{A_{norm}}{A_{\infty}} = K \bullet \sqrt{t} \tag{7}$$

where A/A_{∞} [−] is the released quantity at time t [s], and K [$s^{-1/2}$]is the Higuchi constant, which is related to the rate of diffusion (higher K means faster diffusion). Plotting the released dye quantities as a function of the square root of time, two linear sections can be fitted in the curves (one at the initial burst release stage and one at the later stage, see Fig. 5b and Fig. A9b in Appendix). The values of the parameters fitted to the release curves for the selected samples are summarized in Table 3.

From the data in Table 3, it can be seen that the n value of the Korsmeyer-Peppas model is around 0.5 for all CS-coated systems impregnated at pH 7.4, which means that the CS coating is able to regulate the dye release and diffusion control is achieved in the systems. However, in the case of the bare $pSiO_2$ coating, and the CS-coated systems impregnated at pH 8.8, the n value is above 0.5, and the R^2 value characterizing the applicability of the model is smaller.

The release curves in Fig. 5b and the parameters of the fitted Higuchi model also show that in the case of systems impregnated at a more alkaline pH, diffusion is much faster in the initial stage (more definite burst release, larger slope in Fig. 5b, higher K_1 value), and then the process slows down similarly to the bare $pSiO_2$ coating (small slope and low K_2 value). In contrast, in the case of systems impregnated at pH 7.4, diffusion is much slower in the initial stage (smaller slope, lower K_1 value), and this does not decrease to such an extent in the later stage either (K_2 values), resulting in a more uniform and overall slower release. See the release curve of the (pH 7.4, 22 °C) sample in Fig. 5b. This again emphasizes that although the release conditions are the same, the impregnation conditions fundamentally determine the kinetics of dye release. This is not simply because of the differences in the initial dye concentration: the amount of dye adsorbed at the (pH 8.8, 12 °C) sample is smaller than at the (pH 7.4, 32 °C) sample, yet significantly faster release is observed in the former case.

Presumably, during impregnation at pH 8.8, the structure of the $pSiO_2$ coating (reactive reservoir) may change (small dissolution and precipitation, ripening process), which causes the pore sizes to increase, enabling a more significant burst release, which the CS coating cannot regulate in the release stage. By changing the impregnation conditions, this effect can be tuned, achieving a more pronounced burst release or slower, even release.

4. Conclusions

Accumulation and release of R6G dye molecules were studied by using a bilayer (mesoporous silica/chitosan) coating in aqueous buffer solutions to model the behaviour of nanolayer-type drug delivery systems containing cationic drugs. The cationic dye molecules penetrated the chitosan nanolayer and mainly adsorbed in the mesoporous silica sublayer. Increasing the pH of the loading solution an increased amount of dye accumulated in the porous silica via a coupled equilibrium between the layers and the loading solution. This is indirect evidence that increasing the pH of the impregnating liquid increased the negative charge density of the pore walls. In extreme cases, the solvent can widen the pores through a kind of pseudomorphic transformation, [58,59] and the dye molecules in the pores can presumably facilitate this process as a structure directing agent, which favors the burst release of the active ingredient at the beginning of the process. Though the chitosan nanolayer could moderate the effect of the alkaline medium on the silica pore walls, at the highest investigated pH (8.8) and elevated temperature (32 °C) erosion of silica can occur that manifested itself in desorption of dye molecules. Hence, chitosan on the silica layer directly influences the time evolution of the release (extending the slow stage of that), but also indirectly during the uptake process, as it protects the pore system from damage under, especially, more alkaline conditions. At maximum protection this biopolymer layer can eliminate the burst release stage of the process.

Summarizing, the most important finding of this work is that by using the same two-layer coating for drug uptake and release, drug release can be influenced by the conditions of uptake provided that the reservoir containing the drug chemically interacts with the drug solvent

Table 3
Fitted kinetic model parameters (for the notation and dimensions, see text) and R^2 values for the dye release curves plotted in Fig. 5. Higuchi 1 gives the parameters of the Higuchi-model fitted to the initial stage, while Higuchi 2 gives the parameters of the Higuchi-model fitted to the later stage of the release (the release curves were measured at 25 °C and pH 7.4). (Mean ± standard deviation, $n = 3$, the uppercase letters indicate significant differences in each row, where a common letter means that the two data values are not significantly different).

Kinetic models/Impregnation conditions		$pSiO_2$ pH = 8.8 T = 22 °C	$pSiO_2$/CS pH = 7.4 T = 22 °C	$pSiO_2$/CS pH = 7.4 T = 32 °C	$pSiO_2$/CS pH = 8.8 T = 12 °C	$pSiO_2$/CS pH = 8.8 T = 22 °C
Korsmeyer-Peppas	$10^3 \bullet K_{KP}$	9.8 ± 3.5^{a}	11.9 ± 4.1^{a}	7.8 ± 1.4^{a}	5.8 ± 0.8^{a}	7.6 ± 0.3^{a}
	n	0.71 ± 0.09^{a}	0.43 ± 0.03^{b}	0.50 ± 0.02^{b}	0.68 ± 0.1^{a}	0.56 ± 0.01^{ab}
	R^2	0.894 ± 0.033	0.993 ± 0.002	0.990 ± 0.002	0.975 ± 0.007	0.983 ± 0.004
Higuchi 1	$10^3 \bullet K_1$	30.5 ± 2.1^{a}	7.0 ± 1.1^{d}	9.3 ± 0.4^{d}	22.3 ± 0.4^{b}	14.4 ± 0.8^{c}
	R^2	0.914 ± 0.019	0.983 ± 0.003	0.995 ± 0.001	0.987 ± 0.006	0.992 ± 0.003
Higuchi 2	$10^3 \bullet K_2$	0.7 ± 0.1^{c}	3.4 ± 0.4^{a}	2.1 ± 0.1^{b}	0.8 ± 0.1^{c}	1.9 ± 0.3^{b}
	R^2	0.924 ± 0.038	0.972 ± 0.002	0.984 ± 0.003	0.931 ± 0.008	0.987 ± 0.003

during uptake. This offers a new opportunity to fine-tune the time evolution of the release and to develop coating-type drug delivery systems for use in implant technology.

Abbreviations

BR	Britton-Robinson (buffer)
CS	chitosan
DA	degree of acetylation
Gls	glass substrate
P123	Pluronic P123 template
PFO	pseudo-first-order (kinetic model)
PSO	pseudo-second-order (kinetic model)
R6G	rhodamine 6G dye
$pSiO_2$	mesoporous silica
SiO_2	compact silica
SE	spectroscopic ellipsometry
TEOS	tetraethyl orthosilicate
UV–Vis	UV–visible spectroscopy

CRediT authorship contribution statement

Péter Márton: Writing – original draft, Visualization, Methodology, Investigation, Formal analysis, Conceptualization. **Simon Titkó:** Writing – review & editing, Validation, Resources, Investigation, Formal analysis. **András Marton:** Validation, Resources. **Bálint Fodor:** Writing – review & editing, Validation, Resources, Investigation, Formal analysis. **Péter Basa:** Validation, Resources. **Gergely Stankovits:** Writing – review & editing, Validation, Resources, Investigation, Formal analysis. **Benjámin Gyarmati:** Writing – review & editing, Validation, Resources, Formal analysis. **János Rohonczy:** Writing – review & editing, Validation, Resources, Investigation, Formal analysis. **Tamás Szabó:** Formal analysis, Resources, Validation, Writing – review & editing. **Dániel Zámbó:** Formal analysis, Resources, Validation, Writing – review & editing. **Zoltán Hórvölgyi:** Writing – review & editing, Supervision, Project administration, Methodology, Funding acquisition, Conceptualization.

Declaration of competing interest

The authors declare that they have no known competing financial interests or personal relationships that could have appeared to influence the work reported in this paper.

Acknowledgments

The authors are thankful for Zsombor Pap for the preparation of the samples for the impregnation and release experiments. B. Gyarmati acknowledges the postdoctoral scholarship of BME József Varga Foundation. Projects no. TKP-9-8/PALY-2021 and TKP-6-6/PALY-2021 have been implemented with the support provided by the Ministry of Culture and Innovation of Hungary from the National Research, Development and Innovation Fund, financed under the TKP2021-EGA and TKP2021-NVA funding schemes. Further support was provided by the National Research, Development and Innovation Office via grant FK 138029, EKÖP-25-4-1-BME-132 and STARTING 152904.

Appendix A. Supplementary data

Supplementary data to this article can be found online at https://doi.org/10.1016/j.ijbiomac.2026.151432.

Data availability

Data will be made available on request.

References

[1] A. Bulátkó, A. Domján, J. Madarász, K. László, Interactions in dopamine and indole loaded thermosensitive hydrogels seen by high sensitivity microDSC. Implications for drug delivery, J. Therm. Anal. Calorim. 147 (2022) 11909–11920, https://doi.org/10.1007/s10973-022-11383-8.
[2] P. Kesharwani, A. Bisht, A. Alexander, V. Dave, S. Sharma, Biomedical applications of hydrogels in drug delivery system: an update, J. Drug Delivery Sci. Technol. 66 (2021) 102914, https://doi.org/10.1016/j.jddst.2021.102914.
[3] A. Mammadova, B. Gyarmati, K. Sárdi, A. Paudics, Z. Varga, A. Szilágyi, Thiolated cationic poly(aspartamides) with side group dependent gelation properties for the delivery of anionic polyelectrolytes, J. Mater. Chem. B 10 (2022) 5946–5957, https://doi.org/10.1039/D2TB00674J.
[4] B.Á. Szilágyi, B. Gyarmati, E.L. Kiss, M. Budai-Szűcs, A. Misra, E. Csányi, K. László, A. Szilágyi, *In situ* gelation of thiolated poly(aspartic acid) derivatives through oxidant-free disulfide formation for ophthalmic drug delivery, Colloids Surf. B: Biointerfaces 225 (2023) 113254, https://doi.org/10.1016/j.colsurfb.2023.113254.
[5] M. Pourmadadi, A. Farokh, E. Rahmani, A. Shamsabadipour, M.M. Eshaghi, A. Rahdar, L.F.R. Ferreira, Porous alumina as potential nanostructures for drug delivery applications, synthesis and characteristics, J. Drug Delivery Sci. Technol. 77 (2022) 103877, https://doi.org/10.1016/j.jddst.2022.103877.
[6] S.-R. Li, F.-Y. Huo, H.-Q. Wang, J. Wang, C. Xu, B. Liu, L.-L. Bu, Recent advances in porous nanomaterials-based drug delivery systems for cancer immunotherapy, J. Nanobiotechnol. 20 (2022) 277, https://doi.org/10.1186/s12951-022-01489-4.
[7] Á.F. Szőke, G.S. Szabó, Z. Hórvölgyi, E. Albert, A.G. Végh, L. Zimányi, L. M. Muresan, Accumulation of 2-Acetylamino-5-mercapto-1,3,4-thiadiazole in chitosan coatings for improved anticorrosive effect on zinc, Int. J. Biol. Macromol. 142 (2020) 423–431, https://doi.org/10.1016/j.ijbiomac.2019.09.114.

[8] N. Morin-Crini, E. Lichtfouse, G. Torri, G. Crini, Applications of chitosan in food, pharmaceuticals, medicine, cosmetics, agriculture, textiles, pulp and paper, biotechnology, and environmental chemistry, Environ. Chem. Lett. 17 (2019) 1667–1692, https://doi.org/10.1007/s10311-019-00904-x.
[9] F.S. Rezaei, F. Sharifianjazi, A. Esmaeilkhanian, E. Salehi, Chitosan films and scaffolds for regenerative medicine applications: a review, Carbohydr. Polym. 273 (2021) 118631, https://doi.org/10.1016/j.carbpol.2021.118631.
[10] P.C. McCarthy, Y. Zhang, F. Abebe, Recent applications of dual-stimuli responsive chitosan hydrogel nanocomposites as drug delivery tools, Molecules 26 (2021) 4735, https://doi.org/10.3390/molecules26164735.
[11] Y. Alyassin, E.G. Sayed, P. Mehta, K. Ruparelia, M.S. Arshad, M. Rasekh, J. Shepherd, I. Kucuk, P.B. Wilson, N. Singh, M.-W. Chang, D.G. Fatouros, Z. Ahmad, Application of mesoporous silica nanoparticles as drug delivery carriers for chemotherapeutic agents, Drug Discov. Today 25 (2020) 1513–1520, https://doi.org/10.1016/j.drudis.2020.06.006.
[12] E. Beňová, D. Bergé-Lefranc, V. Zeleňák, M. Almáši, V. Huntošová, V. Hornebecq, Adsorption properties, the pH-sensitive release of 5-fluorouracil and cytotoxicity studies of mesoporous silica drug delivery matrix, Appl. Surf. Sci. 504 (2020) 144028, https://doi.org/10.1016/j.apsusc.2019.144028.
[13] S. Wang, H. Li, Structure directed reversible adsorption of organic dye on mesoporous silica in aqueous solution, Microporous Mesoporous Mater. 97 (2006) 21–26, https://doi.org/10.1016/j.micromeso.2006.08.005.
[14] S. Bhattacharyya, H. Wang, P. Ducheyne, Polymer-coated mesoporous silica nanoparticles for the controlled release of macromolecules, Acta Biomater. 8 (2012) 3429–3435, https://doi.org/10.1016/j.actbio.2012.06.003.
[15] K. Saini, R. Bandyopadhyaya, Transferrin-conjugated polymer-coated mesoporous silica nanoparticles loaded with gemcitabine for killing pancreatic Cancer cells, ACS Appl. Nano Mater. 3 (2020) 229–240, https://doi.org/10.1021/acsanm.9b01921.
[16] C. Liu, J. Guo, W. Yang, J. Hu, C. Wang, S. Fu, Magnetic mesoporous silica microspheres with thermo-sensitive polymer shell for controlled drug release, J. Mater. Chem. 19 (2009) 4764, https://doi.org/10.1039/b902985k.
[17] M. Dabóczi, E. Albert, E. Agócs, M. Kabai-Faix, Z. Hórvölgyi, Bilayered (silica–chitosan) coatings for studying dye release in aqueous media: the role of chitosan properties, Carbohydr. Polym. 136 (2016) 137–145, https://doi.org/10.1016/j.carbpol.2015.09.025.
[18] Á. Szegedi, P. Shestakova, I. Trendafilova, J. Mihayi, I. Tsacheva, V. Mitova, M. Kyulavska, N. Koseva, D. Momekova, S. Konstantinov, H.A. Aleksandrov, P. St Petkov, I.Z. Koleva, G.N. Vayssilov, M. Popova, Modified mesoporous silica nanoparticles coated by polymer complex as novel curcumin delivery carriers, J. Drug Delivery Sci. Technol. 49 (2019) 700–712, https://doi.org/10.1016/j.jddst.2018.12.016.
[19] N.S. Elbialy, S.F. Aboushoushah, B.F. Sofi, A. Noorwali, Multifunctional curcumin-loaded mesoporous silica nanoparticles for cancer chemoprevention and therapy, Microporous Mesoporous Mater. 291 (2020) 109540, https://doi.org/10.1016/j.micromeso.2019.06.002.
[20] H. Tang, J. Guo, Y. Sun, B. Chang, Q. Ren, W. Yang, Facile synthesis of pH sensitive polymer-coated mesoporous silica nanoparticles and their application in drug delivery, Int. J. Pharm. 421 (2011) 388–396, https://doi.org/10.1016/j.ijpharm.2011.10.013.
[21] K.K. Bansal, D.K. Mishra, A. Rosling, J.M. Rosenholm, Therapeutic potential of polymer-coated mesoporous silica nanoparticles, Appl. Sci. 10 (2019) 289, https://doi.org/10.3390/app10010289.
[22] D. Doveiko, K. Kubiak-Ossowska, Y. Chen, Impact of the crystal structure of silica nanoparticles on rhodamine 6G adsorption: a molecular dynamics study, ACS Omega (2024) acsomega.3c06657, https://doi.org/10.1021/acsomega.3c06657.
[23] C. Wang, X. Zhang, S. Liu, Synthesis of transparent silica microspheres with mesopores to encapsulate dye molecules for the fluorescence enhancement, J. Non-Cryst. Solids 596 (2022) 121888, https://doi.org/10.1016/j.jnoncrysol.2022.121888.
[24] P.-Y. Chiu, J.-K. Chen, C.-C. Cheng, Electrostatically driven supramolecular drug-carrier system for targeted, efficient, safer cancer chemotherapy, J. Colloid Interface Sci. 700 (2025) 138360, https://doi.org/10.1016/j.jcis.2025.138360.
[25] Y.-T. Liao, K.C.-W. Wu, J. Yu, Synthesis of mesoporous silica nanoparticle-encapsulated alginate microparticles for sustained release and targeting therapy, J Biomed Mater Res B Appl Biomater (2013), https://doi.org/10.1002/jbm.b.33007.
[26] T. Aydemir, L. Liverani, J.I. Pastore, S.M. Ceré, W.H. Goldmann, A.R. Boccaccini, J. Ballarre, Functional behavior of chitosan/gelatin/silica-gentamicin coatings by electrophoretic deposition on surgical grade stainless steel, Mater. Sci. Eng. C 115 (2020) 111062, https://doi.org/10.1016/j.msec.2020.111062.
[27] P. Zhao, H. Liu, H. Deng, L. Xiao, C. Qin, Y. Du, X. Shi, A study of chitosan hydrogel with embedded mesoporous silica nanoparticles loaded by ibuprofen as a dual stimuli-responsive drug release system for surface coating of titanium implants, Colloids Surf. B: Biointerfaces 123 (2014) 657–663, https://doi.org/10.1016/j.colsurfb.2014.10.013.
[28] L. Heux, J. Brugnerotto, J. Desbrières, M.-F. Versali, M. Rinaudo, Solid state NMR for determination of degree of acetylation of chitin and chitosan, Biomacromolecules 1 (2000) 746–751, https://doi.org/10.1021/bm000070y.
[29] M.R. Kasaai, Determination of the degree of N-acetylation for chitin and chitosan by various NMR spectroscopy techniques: a review, Carbohydr. Polym. 79 (2010) 801–810, https://doi.org/10.1016/j.carbpol.2009.10.051.
[30] N. Balázs, P. Sipos, Limitations of pH-potentiometric titration for the determination of the degree of deacetylation of chitosan, Carbohydr. Res. 342 (2007) 124–130, https://doi.org/10.1016/j.carres.2006.11.016.
[31] N. Yan, X.-F. Wan, X.-S. Chai, Rapid determination of degree of deacetylation of chitosan by a headspace analysis based titrimetric technique, Polym. Test. 76 (2019) 340–343, https://doi.org/10.1016/j.polymertesting.2019.03.034.
[32] M. Ali, M. Shakeel, K. Mehmood, Extraction and characterization of high purity chitosan by rapid and simple techniques from mud crabs taken from Abbottabad, Pak. J. Pharm. Sci. 32 (1) (2019) 171–175.
[33] P. Sorlier, C. Viton, A. Domard, Relation between solution properties and degree of acetylation of chitosan: role of aging, Biomacromolecules 3 (2002) 1336–1342, https://doi.org/10.1021/bm0256146.
[34] L.C. Wang, X.G. Chen, C.S. Liu, P.W. Li, Y.M. Zhou, Dissociation behaviors of carboxyl and amine groups on carboxymethyl-chitosan in aqueous system, J. Polym. Sci. Part B Polym. Phys. 46 (2008) 1419–1429, https://doi.org/10.1002/polb.21475.
[35] Q.Z. Wang, X.G. Chen, N. Liu, S.X. Wang, C.S. Liu, X.H. Meng, C.G. Liu, Protonation constants of chitosan with different molecular weight and degree of deacetylation, Carbohydr. Polym. 65 (2006) 194–201, https://doi.org/10.1016/j.carbpol.2006.01.001.
[36] B. Tegze, E. Albert, B. Dikó, N. Nagy, A. Rácz, G. Sáfrán, A. Sulyok, Z. Hórvölgyi, Effect of silver modification on the Photoactivity of Titania coatings with different pore structures, Nanomaterials 11 (2021) 2240, https://doi.org/10.3390/nano11092240.
[37] P. Márton, Ö.T. Nagy, D. Kovács, B. Szolnoki, J. Madarász, N. Nagy, G.S. Szabó, Z. Hórvölgyi, Barrier behaviour of partially N-acetylated chitosan layers in aqueous media, Int. J. Biol. Macromol. 232 (2023) 123336, https://doi.org/10.1016/j.ijbiomac.2023.123336.
[38] E. Hild, A. Deák, L. Naszályi, Ö. Sepsi, N. Ábrahám, Z. Hórvölgyi, Use of the optical admittance function and its WKB approximation to simulate and evaluate transmittance spectra of graded-index colloidal films, J. Opt. A Pure Appl. Opt. 9 (2007) 920, https://doi.org/10.1088/1464-4258/9/10/023.
[39] E. Albert, P. Basa, B. Fodor, Z. Keresztes, J. Madarász, P. Márton, D. Olasz, A. S. Rácz, G. Sáfrán, T. Szabó, B. Tegze, T. Höltzl, Z. Hórvölgyi, Experimental and computational synthesis of TiO2 sol–gel coatings, Langmuir 41 (2025) 704–718, https://doi.org/10.1021/acs.langmuir.4c03959.
[40] D. Lan, H. Zhu, J. Zhang, S. Li, Q. Chen, C. Wang, T. Wu, M. Xu, Adsorptive removal of organic dyes via porous materials for wastewater treatment in recent decades: a review on species, mechanisms and perspectives, Chemosphere 293 (2022) 133464, https://doi.org/10.1016/j.chemosphere.2021.133464.
[41] A. Ábrahám, L. Kócs, E. Albert, B. Tegze, B. Szolnoki, N. Nagy, G. Sáfrán, P. Basa, Z. Hórvölgyi, Durability of microporous hybrid silica coatings: optical and wetting properties, Thin Solid Films 699 (2020) 137914, https://doi.org/10.1016/j.tsf.2020.137914.
[42] L. Kócs, E. Albert, B. Tegze, M. Kabai-Faix, C. Major, A. Szalai, P. Basa, Z. Hórvölgyi, Silica sol-gel coatings with improved light transmittance and stability, Period. Polytech. Chem. Eng. 62 (2017) 21–31, https://doi.org/10.3311/PPch.10550.
[43] W.M. Facchinatto, D.M. dos Santos, A. Fiamingo, R. Bernardes-Filho, S. P. Campana-Filho, E.R. de Azevedo, L.A. Colnago, Evaluation of chitosan crystallinity: a high-resolution solid-state NMR spectroscopy approach, Carbohydr. Polym. 250 (2020) 116891, https://doi.org/10.1016/j.carbpol.2020.116891.
[44] J. Weißpflog, D. Vehlow, M. Müller, B. Kohn, U. Scheler, S. Boye, S. Schwarz, Characterization of chitosan with different degree of deacetylation and equal viscosity in dissolved and solid state – insights by various complimentary methods, Int. J. Biol. Macromol. 171 (2021) 242–261, https://doi.org/10.1016/j.ijbiomac.2021.01.010.
[45] J. Dutta, Priyanka, A facile approach for the determination of degree of deacetylation of chitosan using acid-base titration, Heliyon 8 (2022) e09924, https://doi.org/10.1016/j.heliyon.2022.e09924.
[46] Z. Deng, T. Wang, X. Chen, Y. Liu, Applications of chitosan-based biomaterials: a focus on dependent antimicrobial properties, Mar. Life Sci. Technol. 2 (2020) 398–413, https://doi.org/10.1007/s42995-020-00044-0.
[47] G. Ruiz-Pulido, D. Quintanar-Guerrero, L.E. Serrano-Mora, D.I. Medina, Triborheological analysis of reconstituted gastrointestinal mucus/chitosan:TPP nanoparticles system to study Mucoadhesion phenomenon under different pH conditions, Polymers 14 (2022) 4978, https://doi.org/10.3390/polym14224978.
[48] S. Valetti, A. Feiler, M. Trulsson, Bare and effective charge of mesoporous silica particles, Langmuir 33 (2017) 7343–7351, https://doi.org/10.1021/acs.langmuir.7b01135.
[49] J. Cho, M.-C. Heuzey, A. Bégin, P.J. Carreau, Physical gelation of chitosan in the presence of β-Glycerophosphate: the effect of temperature, Biomacromolecules 6 (2005) 3267–3275, https://doi.org/10.1021/bm050313s.
[50] C.-H. Huang, K.-P. Chang, H.-D. Ou, Y.-C. Chiang, C.-F. Wang, Adsorption of cationic dyes onto mesoporous silica, Microporous Mesoporous Mater. 141 (2011) 102–109, https://doi.org/10.1016/j.micromeso.2010.11.002.
[51] F. López Arbeloa, V. Martínez Martínez, T. Arbeloa, I. López Arbeloa, Photoresponse and anisotropy of rhodamine dye intercalated in ordered clay layered films, J. Photochem. Photobiol. C Photochem. Rev. 8 (2007) 85–108, https://doi.org/10.1016/j.jphotochemrev.2007.03.003.
[52] B. Tegze, E. Albert, B. Fodor, G. Sáfrán, Z. Hórvölgyi, Photoinduced processes of adsorbed and associated dye molecules in mesoporous titania coatings, Dyes Pigments 167 (2019) 109–119, https://doi.org/10.1016/j.dyepig.2019.04.017.
[53] H. Douba, O. Mohammedi, B. Cheknane, Adsorption of rhodamine 6G dye onto Al-MCM-41 and MCM-41 mesoporous materials, Kem. U Ind. (2022), https://doi.org/10.15255/KUI.2022.001.
[54] M. Vallet-Regí, F. Balas, D. Arcos, Mesoporous materials for drug delivery, Angew. Chem. Int. Ed. 46 (2007) 7548–7558, https://doi.org/10.1002/anie.200604488.

[55] M. Jarosz, A. Pawlik, M. Szuwarzyński, M. Jaskuła, G.D. Sulka, Nanoporous anodic titanium dioxide layers as potential drug delivery systems: drug release kinetics and mechanism, Colloids Surf. B: Biointerfaces 143 (2016) 447–454, https://doi.org/10.1016/j.colsurfb.2016.03.073.

[56] M.P. Paarakh, J. Preethy Ani, S. CM, P.G. V., Release kinetics - concepts and applications, Int. J. Pharm. Res. Technol. 8 (2019), https://doi.org/10.31838/ijprt/08.01.02.

[57] T. Higuchi, Mechanism of sustained-action medication. Theoretical analysis of rate of release of solid drugs dispersed in solid matrices, J. Pharm. Sci. 52 (1963) 1145–1149, https://doi.org/10.1002/jps.2600521210.

[58] M. Boudot, V. Gaud, M. Louarn, M. Selmane, D. Grosso, Sol–gel based hydrophobic antireflective coatings on organic substrates: a detailed investigation of ammonia vapor treatment (AVT), Chem. Mater. 26 (2014) 1822–1833, https://doi.org/10.1021/cm403787v.

[59] A.M. Bors, J. Madarász, N. Nagy, A.S. Rácz, G. Sáfrán, D. Olasz, Z. Hórvölgyi, E. Albert, Ammonia vapor-induced pseudomorphic transformation of mesoporous TiO2 sol–gel coatings, ACS Omega 10 (2025) 35029–35042, https://doi.org/10.1021/acsomega.5c04483.